Spectrally selective thermal radiators and absorbers with periodic microstructured surface for high temperature applications

Hitoshi Sai and Hiroo Yugami

Department of Machine Intelligence and Systems Engineering, Tohoku University, Aoba01, Aramaki, Aoba-ku, Sendai, 980-8579, Japan

Yoshiaki Kanamori and Kazuhiro Hane

Department of Mechatronics and Precision Engineering, Tohoku University, Aoba01, Aramaki, Aoba-ku, Sendai, 980-8579, Japan

Summary

Spectral absorptance and emittance of W surface gratings with short periodicity corresponding to the VIS to NIR wavelengths has been investigated to develop spectrally selective devices for high-temperature applications such as selective solar absorbers and selective radiators for thermophotovoltaic systems. Numerical calculations based on rigorous coupled-wave analysis have been performed to evaluate the grating parameters. Two kinds of W surface gratings composed by microcavities have been fabricated by fast atom beam etching with two different lithography techniques. These gratings have shown strong absorption or emission due to the surface microstructures in the VIS to NIR region, whereas their reflectance in the IR region is kept at a high level. Their high thermal stability is confirmed from heating tests under vacuum or reduced atmospheres. Physical aspect of the interaction of electromagnetic wave with lossy gratings has been also discussed briefly.

1. Introduction

It is well known that optical properties of materials depend on not only the intrinsic characteristics but also their surface morphology. For example, rough surfaces display lower reflectance or higher absorptance than that of polished surfaces. When periodical microstructures are processed on material surfaces, what is known as surface gratings, optical properties are affected by geometrical parameters like periodicity, aperture, depth, and so on. If the geometrical dimensions are close to the wavelengths of lights in particular, curious phenomena such as Wood anomalies (Wood (1902)) can be observed due to the interactions of electromagnetic waves with surface microstructures.

One of the advantages of optical control by surface gratings is high thermal stability of optical devices, because they are usually fabricated on bulk materials and therefore there is no thermal discontinuity inside them unlike to multiple coatings. This means that spectral control with surface gratings is very efficient for high-temperature applications. Hesketh et al. (1986) and Zemel (1988) have reported on spectral thermal emittance from one-dimensional (1D) Si surface gratings. They have shown the several emittance peaks due to the resonance between electromagnetic radiation and surface gratings whose dimensions are comparable with wavelengths in the infrared (IR) region. Owing to recent developments of micromaching technique, it has been possible to fabricate surface microstructures whose dimensions are close to the visible (VIS) or near IR (NIR) wavelengths with good accuracy. Heinzel et al. (2000) and Sai et al. (2001) have demonstrated that 2D surface metallic gratings in the NIR region can control thermal emittance spectra. Their reports show the possibility that surface microstructures can be utilized for spectral control at high temperatures.

In this study, we have researched on the optical properties of metallic surface gratings with two different periods, 0.5 and 1.0 μm, in order to produce spectrally selective thermal devices. The former is a selective solar absorber aiming at efficient photothermal conversion at high temperatures, and the latter is a selective thermal radiator for raising the efficiency of thermophotovoltaic (TPV) generation (Coutts (1999)). We choose W as a substrate material because of its very high melting point and intrinsic absorption in the VIS to NIR region.

Figure 1 (a) shows the normalized solar spectrum under the air mass of 1.5 reported by Japanese Industrial Standard Committee (1998) and the spectral absorptance α_λ of an ideal selective solar absorber for high-temperature applications (>1000K). Although various kinds of selective absorbers have been

commercialized until now, most of them are designed for low temperature (<500K) applications, because their spectral selectivity and thermal stability are low. We have developed new selective absorber surfaces suited for high-temperature use by means of W surface gratings.

Figure 1 (b) shows the spectral response of several compound photovoltaic (PV) cells utilized in TPV applications (Coutts (1998)) and the spectral emittance ε_λ curve of an ideal selective radiator. In TPV generation systems, thermal radiation from radiators heated at a high temperature converts into electricity with narrow bandgap PV cells. Selective radiators, whose emittance is high within PV cell's sensitive region and low outside it, have been studied to raise the efficiency of TPV systems. There are several methods to obtain selective radiator (Coutts, (1999)), but sufficient properties had not been achieved yet. We have developed selective radiator surfaces suitable for TPV systems with W surface gratings.

As a first step to obtain the optimum design for selective surfaces with 2D gratings, we have conducted numerical calculations with rigorous coupled wave analysis (RCWA) (Moharam (1988)) algorithm. Based on the calculated results, we have fabricated 2D W surface gratings with microcavities by fast atom beam (FAB) etching (Toma et al. (1997)). We have used two different lithographic techniques, namely, highly ordered porous alumina membrane and electron beam lithography. Successive measurements of spectral reflectance and emittance have indicated that W surface gratings display spectral selectivity. A heating test under a vacuum atmosphere has been also conducted and it has proved that W gratings have high thermal stability.

2. Calculation method

We have performed RCWA calculation (Moharam (1988), Peng & Morris (1995), Kanamori et al. (2000)) to simulate the optical properties of the microstructured surfaces. RCWA is a method to analyze the general 3D grating diffraction problem by solving Maxwell's equations rigorously. Input data are only the state of incident beam, structural profiles, and optical constants (n, k) of materials. Diffraction efficiency for each diffraction order is determined through RCWA. We consider the diffraction orders up to ±7th for x- and y- directions, respectively, and therefore diffraction efficiencies for 225 diffraction orders are calculated for each wavelength. We have checked the calculation outputs sufficiently converge under these conditions. The optical constants of W reported by Lynch & Hunter (1985) are used in the calculation.

Figure 2 shows schematic diagram of RCWA calculation. Here we define some parameters to

describe surface microstructures and the state of incident wave. Λ, a and d denote the structural periodicity, aperture size, and depth, respectively. In this study, we set $\Lambda_x = \Lambda_y = \Lambda$ and $a_x = a_y = a$. Incident angle θ and azimuthal angle ϕ are defined as shown in the figure. Polarization angle is defined as $\psi = \tan^{-1}(A_s/A_p)$, where A_s and A_p denote the amplitudes of the *s*- and *p*- polarization components of the incident wave, respectively.

3. Experimental setup

We have evaluated the spectral features of W surface gratings through optical measurements. The optical spectra for 0.2 to 5.0μm are measured with two kinds of spectrometers, namely, a grating spectrometer (Perkin-Elmer, Lambda 900) for the VIS and NIR region and a Fourier-transform spectrometer (FTIR) (Perkin-Elmer, GX2000) for the IR region. An Al mirror whose spectral reflectance has previously known is used as a reference. For measuring α_λ rigorously, an integral sphere is used to measure the all reflectance components distributed in a hemispherical space. Instead of the integral sphere, in this study, we have used a diffuse reflectance geometry, which can collect the reflected lay within about ± 20° from the center angle. The incident beam enters to the sample at 30° and polarizes randomly.

For measuring ε_λ, we have built up the apparatus equipped with a micro heater (LINKAM, TS-1500) and the FTIR with an emission port. Thermal emission from a sample surface is led to the emission port with two CaF_2 lenses and a pinhole, and analyzed by the FTIR. The measured spectra are calibrated and given units by comparing with the emissive spectra of the materials whose emittance has been already known, for example, SiC. Sample temperatures have been determined with a radiation thermometer by measuring the temperature of a flat W substrate heated simultaneously with microstructured samples. During measurements, Ar + 5% H_2 gas is flown inside the heater casing to prevent samples from oxidation.

4. Selective Solar Absorber

4.1. Calculation

Demanded characteristics for selective solar absorbers are high solar absorbance, low thermal emittance, environmental durability, and so on. The angular-dependent solar absorptance α_s, thermal

emittance ε are usually defined by following equations (Zhang, (2000)),

$$\alpha_s(\theta) = \frac{\int_0^\infty \alpha_\lambda(\lambda,\theta) E_s(\lambda) d\lambda}{\int_0^\infty E_s(\lambda) d\lambda}, \quad (1)$$

$$\varepsilon(\theta) = \frac{\int_0^\infty \varepsilon_\lambda(\lambda,\theta) E_b(T,\lambda) d\lambda}{\int_0^\infty E_b(T,\lambda) d\lambda}. \quad (2)$$

Here, $E_s(\lambda)$ is the spectral solar irradiance, $E_b(T, \lambda)$ is the spectral emissive power of black body at the temperature of T, and λ is wavelength. To achieve high photothermal conversion efficiency, high α_s is essential regardless of operating temperatures, whereas contribution of low ε becomes more significant with increasing temperature since thermal radiation loss is proportional to εT^4.

We have calculated the spectral feature of W surface gratings varying structural parameters to search the optimum design realizing high α_s and low ε simultaneously. Figure 3 shows the absorptance spectra of W surface gratings with rectangular microcavities with $a/\Lambda = 0.8$ and $d/a = 1.0$. θ, ϕ and ψ of the incident beam are all set to 0°. All of the W gratings display pronounced α_λ peaks in the range of $0.3 < \lambda < 2.0$ μm with keeping low α_λ in the IR wavelengths. It is found that the cut off wavelength becomes longer gradually with increasing Λ. α_λ of a black Ni absorber (Wäckelgård (1998)), which is one of the most popular selective coatings, is also drawn in the figure. Comparing with the black Ni, the sharp change on α_λ at the NIR region is more suitable for selective solar absorbers for high-temperature applications. In addition, not shown as a figure, calculations have clarified that the spectral feature of W surface gratings with microcavities is insensitive to θ, especially for $\theta < 60°$. This is a preferable characteristic for a solar absorber.

From the computed absorptance spectra with various parameters, we have calculated α_s and ε of W surface gratings with eqs. (1) and (2). The solar spectrum shown in Fig. 1 (a) is used as $E_s(\lambda)$ in the calculations. In calculating ε, it has been supposed that ε_λ is equal to α_λ based on Kirchhoff's low, and has no temperature dependence. The calculated α_s is potted in Fig. 4 as a function of Λ for three different d/a conditions by the solid lines with marks. It can be found that $\alpha_s \sim 0.85$ is obtained for $\Lambda > 0.5$ μm and $d/a > 1.0$. As a whole, α_s rises with increasing Λ or d/a, but its gain is not conspicuous for $\Lambda > 0.5$ μm or $d/a > 1.0$. Calculated ε at two different temperatures are also plotted in Fig. 4. ε of W surface gratings is

sufficiently restrained at low temperatures (ε < 0.04 at 400K), and it still remains low level at elevated temperatures. For instance, ε = 0.061 at 800K and 0.137 at 1200K are obtained for Λ = 0.5 μm, a/Λ = 0.8, and d/a = 1.0.

4.2. Sample Preparation

In the previous section, it has been confirmed by numerical calculation that the 2D W surface gratings with Λ ~ 0.5 μm, a/Λ ~ 0.8, and d/a > 1.0 has a good spectral selectivity suitable for using as a high-temperature selective absorber. To demonstrate that experimentally, we have fabricated 2D surface gratings with submicron holes on bulk-W substrates by means of FAB etching technique (Toma et al. (1997)). Since FAB is electrically neutral atomic or molecular beam, it is possible to obtain fine patterns with nanometer order without deformation of etching shape due to accumulated charge on samples. As an etching mask, we have used highly ordered porous alumina membrane (Li et al. (1998), Masuda et al. (1998), Masuda et al. (1996)). Self-ordering of the pores into a honeycomb arrangement occurs at several appropriate conditions during anodization. Thereby nano-scale periodic structures can be processed in a large area at low cost by using porous alumina. In the fabrication of porous alumina membranes, we have referred to the anodization condition reported by Masuda et al. (1998) to obtain an etching mask with Λ = 0.5 μm.

The fabrication process in this study is similar to that of our previous report (Kanamori et al. (2001)). In the preparation of porous alumina masks, we use two-step anodizing process reported by Masuda et al. (1996). First, highly ordered porous alumina membrane is formed on an electrochemically polished Al sheet (99.999%) with 0.2 mol/l phosphoric acid at the voltage of 195V and 0°C by the two step anodization. Next, the alumina film is separated out from the Al sheet by soaking in a saturated $HgCl_2$ solution. Then pore-widening treatment is carried out in 0.5wt% phosphoric acid solution at 40 °C. In the meantime, barrier layer is removed and pores are pierced. Pore diameter can be adjusted by varying the etching time. Putting the alumina mask on a mechanically polished W substrate with the size of 10 × 10 × 0.5 mm, FAB etching with SF_6 gas is performed with the FAB system (EBARA, FAB-60 ML) to replicate the periodic porous arrays on the bulk W. Finally, the remaining mask is taken away in the mixed solution of chromic and phosphoric acid.

Figure 5 shows scanning electron microscope (SEM) images of a W surface grating fabricated by FAB etching at the discharge voltage of 3.0 kV and the SF_6 flow rate of 5.6 SCCM for 40 min. Pore arrangement in honeycomb manner of the alumina mask is well replicated on W surfaces without deformation of the etching pattern. The sample surface is composed of cylindrical cavities with a = 0.45 μm and d ~ 0.3 μm. Viewing in a large scale, it consists of numbers of domains in which pores are orderly placed and disorders near the boundary of them. Although the cavity shape is different from that of the numerical simulations, this surface grating with submicron cavities is expected to show the spectral feature suited for selective solar absorbers.

4.3. Results and Discussion

The diffuse reflectance spectra of the porous W are plotted in Fig. 6. In comparison with a flat W, reflectance of the porous W fairly decreases in the wavelengths shorter than 2.0μm, in spite of keeping high reflectance in the IR region. α_s = 0.82 is obtained from the spectra shown in Fig.6. On the other hand, ε for the angle of 30° are evaluated as 0.057 at 400K, 0.090 at 800K and 0.159 at 1200K. Although these results are slightly worse than those obtained in numerical calculations, it can be proved experimentally that the porous W surfaces realize high α_s and low ε at high temperatures simultaneously.

In the VIS region, W doesn't support surface plasmons because the real part of its dielectric constant is not negative. In addition, the absorption band doesn't become broader with deepening the holes unlike to subwavelength gratings as shown in Fig. 3. Therefore, we consider that this absorption mainly originates from an enhancement of the intrinsic absorption of W by the standing wave resonance due to the submicron holes. This is also supported by the calculation result that the spectral feature of W surface gratings with microcavities is insensitive to θ oppositely to surface plasmon resonances (SPR).

We have performed a thermal stability test at 1170K for 5 h in a vacuum atmosphere under 1×10^{-2} Pa. After the heating, no remarkable changes have been found on the sample surfaces through SEM observations. In addition, the spectral reflectance after the heating is almost same as those of before as shown in Fig. 6. This result has clarified that the porous W surfaces can be applied for selective solar absorbers at as a high temperature as 1170K.

5. Selective Radiator

5.1. Calculation

To develop high-efficiency TPV systems, we need selective emitters whose emittance varies from 0 to 1 at $\lambda \sim 2.0$ μm as shown in Fig. 1(b). Aiming at this spectral feature, we have calculated the spectral feature of W surface gratings in the same way described in section 4.1. Figure 7 shows ε_λ ($=\alpha_\lambda$) of W surface gratings with rectangular cavities under the condition of $\Lambda = 1.0$ μm, $d/a = 1.0$, and $\theta = \phi = \psi = 0°$. ε_λ increases drastically with increasing a/Λ in the shorter wavelengths, whereas it crawls at bottom level in the IR region. This is a suitable property to be applied as selective radiators in TPV systems. For $a/\Lambda = 0.5$ and 0.7 only one dominant peak of ε_λ is clearly observed, while multiple peaks are observed for $a/\Lambda = 0.9$. The cutoff wavelength, at which ε_λ changes sharply, becomes longer with increasing a/Λ. Calculations have clarified that deepening the cavity more than $d/a = 1.0$ is not effective to refine the spectral feature. They have also shown the small angle dependence of ε_λ of W cavities with d/a more than 1.0 as mentioned in the section 3.1.

The design of W surface gratings for selective radiators depends on what kind of PV cells is used in the system. Here, we select GaSb as a TPV cell because it is the cheapest one in the PV cells shown in Fig. 1(b). The sensitive region of GaSb is about 0.6 to 1.7 μm. From the results described above, we choose $\Lambda = 1.0$ μm, $a/\Lambda = 0.8$ and $d/a = 1.0$ as the optimum parameters for selective radiators.

5.2. Sample preparation

For fabrication the W surface gratings with $\Lambda = 1.0$ μm, we have combined electron beam (EB) lithography and FAB etching. First, photo resist layer ($t = 1.5$ μm) is formed on the mechanically polished W substrate. After Al film ($t = 0.1$ μm) is evaporated on it, EB resist is additionally coated ($t = 0.4$ μm) with a spin coater. Then grating pattern is drawn on the top EB resist and developed. Next, FAB etching with SF_6 gas is carried out to replicate the grating pattern to the Al film. After that, FAB etching with O_2 gas is successively carried out to replicate the grating pattern to the photo resist layer. By means of this double layer resist technique, deep resist pattern can be processed on a W substrate. Finally, FAB etching with SF_6 is performed again to replicate the resist pattern to the W surface and the W surface grating with rectangular cavities is fabricated.

Figure 8 shows SEM images of a W surface grating fabricated by the process described above. It is confirmed that rectangular microcavities are formed on a W surface periodically. Although the walls of the cavities are a little tapered and their surface is not flat, geometrical parameters of this sample are evaluated as Λ = 1.0 μm, a ~ 0.8 μm and d ~ 0.8 μm through SEM observations.

5.3. Results and Discussion

Figure 9 displays the diffuse reflectance spectra of the W surface grating shown in Fig. 8. The W grating shows very low reflectance for λ < 2.0 μm with keeping high reflectance for λ > 2.0 μm, and therefore it is expected to possess high ε_λ selectively in the VIS to NIR region. A clear minimum is observed at λ = 1.4 μm and it splits into two minima with increasing ϕ from 0° to 45°. This result suggests that this minimum is affected by the arrangement or periodicity of microcavities. Several structures are also observed for λ < 0.8 μm, but we cannot determine only from Fig. 9 whether they are originated from sort of absorptions or simple diffractions.

Figure 10 shows the measured ε_λ of the W grating shown in Fig. 8 at the normal direction under a reductional atmosphere at 1100K. Measured ε_λ of a flat W is added in the figure as a reference with the literature data (Touloukian DeWitt (1970)). As compared with that of a flat W, ε_λ of the W grating shows a clear peak at λ = 1.3 μm. This peak is corresponded to the minimum shown in Fig. 9, and it satisfies Kirchhoff's law approximately. In detail, however, several differences from Fig.9 are observed: the ε_λ peak value of about 0.7 is smaller that that expected from Fig.9, and the peak wavelength of λ = 1.3 μm is a little shorter than that of the minimum in Fig. 9. We speculate that the main reason of them is the temperature dependence of optical constants. Therefore it is considered that the measurement of optical constants at high temperature is important to understand these phenomena and design the spectral selective radiator

The wavelength of the dominant peak observed in the Fig. 9 and Fig. 10 is much longer than the structural period of Λ = 1.0 μm. In addition, its bandwidth is relatively broad. These are different from the characteristic of SPR, which show a sharp absorption at $\lambda \sim \Lambda$. Moreover, in the wavelength region of 1.0 μm < λ < 1.5 μm, the real part of dielectric constants of W is negative at room temperature but the absolute value is so small that the density of surface plasmons excited on W may be low. From these reasons, it is considered that this absorption and emission peak mainly originates from the standing wave resonance due

to the rectangular microcavities. On the other hand, the dependence of ϕ shown in Fig. 9 may support the contribution from the effect of periodicity. Further investigation is needed for understanding in the detail of these phenomena.

After the measurement of ε_λ, SEM observations and reflectance measurements have been performed to check the thermal stability of the W surface gratings. As the same as the selective solar absorber, we have confirmed that the sample has shown no remarkable alternations before and after the heating.

7. Summary

We have investigated about the spectral properties of W surface gratings with short periodicity corresponding to the VIS to NIR wavelengths. Spectral control of absorption or emission by means of surface gratings has been demonstrated through experiments and numerical calculations, and it has proved that this scheme can be applied to fabricate spectral selective devices for high-temperature applications. Physical aspect of this phenomenon has been also discussed breifly. Further investigation is needed for understanding in the detail. In addition, it has been clarified that the necessity of optical constants at high temperatures for the design of spectral selective devices.

Acknowledgements

A part of this work was supported by Grant-in-Aid for Scientific Research (B) (No.11555057) and JSPS Fellows (No.08440) from The Ministry of Education, Science, Sports and Culture, and by a Grant Program of the Asahi Glass Foundation. This study was carried out as a part of “Ground Research Announcement for Space Utilization” promoted by Japan Space Forum. A part of this work was performed in Venture Business Laboratory in Tohoku University.

References

1. Coutts, T.J. (1999) A review of progress in thermophotovoltaic generation of electricity, **Renewable and Sustainable Energy Reviews**, 3, pp. 77-184.
2. Kanamori, Y., Hane, K., Sai, H. & Yugami, H. (2001) 100nm period silicon antireflection structures fabricated using a porous alumina membrane mask, **Applied Physics Letters**, 78, pp. 142-143.
3. Kanamori, Y., Kikuta H. & Hane, K. (2000) Broadband antireflection gratings for glass substrates fabricated by fast atom beam etching, **Japanese Journal of Applied Physics**, Part 2, 39, pp. L735-L737.
4. Heinzel, A., Boerner, V., Gombert, A., Bläsi, B. & Wittner V., & Luther (2000) Radiation filters and emitters for the NIR based on periodically structured metal surfaces, **Journal of Modern Optics**, 47, pp. 2399-2419.
5. Hesketh, P.J., Zemel, J.N. & Gebhart, B. (1986) Organ pipe radiation resonant mode of periodic micromachined silicon surfaces, **NATURE**, 324, pp. 549-551.
6. Japanese Industrial Standard Committee (1998) Secondary reference crystalline solar cells, in: **Japanese Industrial Standard**, JIS C 8911 (Tokyo, Japanese Standards Association).
7. Li, A.P., Müllar, F., Birner, A., Nielsch, K. & Gösele, U. (1998) Hexagonal pore arrays with a 50-420nm interpore distance formed by self-organization in anodic alumina, **Journal of Applied Physics**, 84, pp. 6023-6026.
8. Lynch, D.W. & Hunter, W.R. (1985) Optical constants of metals, in: Palik, E.D. (Eds) **Handbook of Optical Constants of Solids I**, pp. 334-341 (New York, Academic Press).
9. Masuda, H., Yada, K. & Osaka, A. (1998) Self-ordering of cell configuration of anodic porous alumina with large-size pores in phosphoric acid, **Japanese Journal of Applied Physics**, Part2, 37, pp. L1340-L1342.
10. Masuda, H. & Satoh, M. (1996) Fabrication of gold nanodot array using anodic porous alumina as an evaporation mask, Japanese Journal of Applied Physics, Part2, 35, pp. L126-L129.
11. Moharam, M.G. (1988) Coupled-Wave Analysis of Two-Dimensional Dielectric Gratings, in: **Proceedings of SPIE**, 883, pp. 8-11.
12. Peng, S. & Morris, G.M. (1995) Efficient implementation of rigorous coupled-wave analysis for

surface-relief gratings, **Journal of the Optical Society of America A**, 12, pp. 1087-1096.

13. Sai, H., Yugami, H., Kanamori, Y. & Hane, K. (2001) Spectral control of thermal emission by periodic microstructured surfaces in the near-infrared region, **Journal of the Optical Society of America A**, 18, pp. 1471-1476.
14. Toma, Y., Hatakeyama, M., Ichiki, K., Huang, J., Yamaguchi, K., Watanabe, K. & Kato, T., (1997) Fast atom beam etching of glass materials with contact and non-contact masks, **Japanese Journal of Applied Physics**, 36, pp. 7655-7659.
15. Touloukian, Y.S. & DeWitt, D.P. (Eds) (1970) **Thermal Radiative Properties Metallic Elements and Alloys**, pp. 776-826 (New York , IFI/Plenum).
16. Wäckelgård, E. (1998) Characterization of black nickel solar absorber coatings electroplated in a nickel chlorine aqueous solution, **Solar Energy Materials & Solar Cells**, 56, pp. 35-44.
17. Wood, R.W. (1902) On a Remarkable Case of Uneven Distribution of Light in a Diffraction Grating Spectram, **Philosophical Magazine**, 4, pp. 396-402.
18. Zemel, J.N. (1988) Black Body Radiation and Transport Processes from Microstructure, **Comments on Condensed Matter Physics**, 14, pp. 1-20.
19. Zhang, Q.-C. (2000) Recent progress in high-temperature solar selective coatings, **Solar Energy Materials & Solar Cells**, 62, pp. 63-74.

Figure Captions

Fig. 1. (a) Comparison of the solar spectrum and an ideal spectral feature of selective solar absorbers. (b) Comparison of spectral responses of several PV cells and an ideal spectral feature of selective radiators for TPV applications.

Fig. 2. Schematic diagram of the calculation model.

Fig. 3. Calculated α_λ of the W surface gratings with rectangular cavities with a/Λ = 0.8, d/a = 1.0 and measured α_λ of black nickel reported by Wäckelgård (1998). The state of the incident beam is $\theta = \phi = \psi =$ 0° in the calculation.

Fig. 4. Calculated normal α_s and ε of the W surface grating with rectangular cavities.

Fig. 5. SEM images of the top view (left) and oblique view (right) of the W surface gratings fabricated with an ordered porous alumina membrane mask and FAB etching.

Fig. 6. Measured diffuse reflectance spectra of the 2D W surface grating shown in fig. 5 before and after a heating test up to 1170K in a vacuum atmosphere.

Fig. 7. Calculated ε_λ (α_λ) of the W surface gratings with rectangular cavities with Λ = 1.0 μm, d/a = 1.0 and measured. The state of the incident beam is $\theta = \phi = \psi = 0°$ in the calculation.

Fig. 8. SEM images of the top view (left) and oblique view (right) of the W surface gratings with rectangular microcavities fabricated with EB lithography and FAB etching.

Fig. 9. Measured diffuse reflectance spectra of the 2D W surface grating shown in fig. 8 at two different ϕ, 0° and 45°.

Fig. 10. Measured normal ε_λ of the W surface grating shown in Fig. 8 at 1100K.

Fig. 1.

Sai et al.

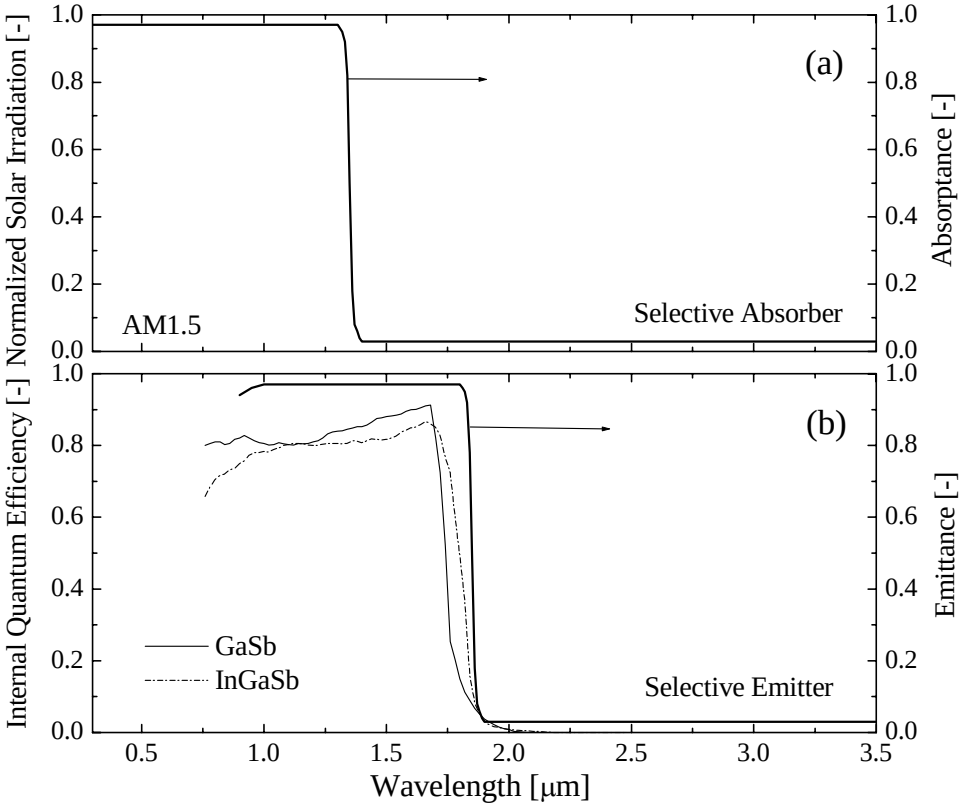

Fig. 2.

Sai et al.

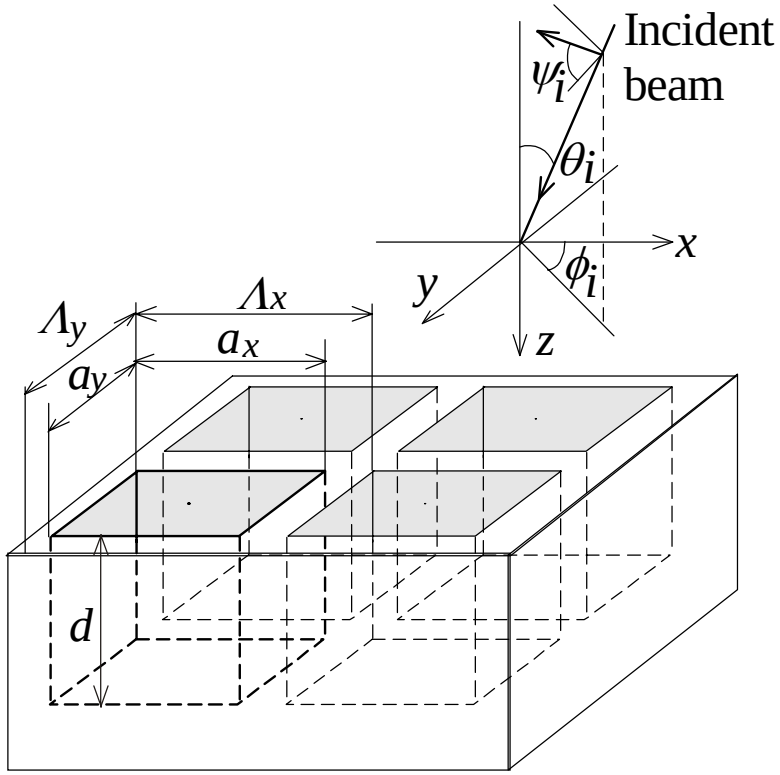

Fig. 3.

Sai et al.

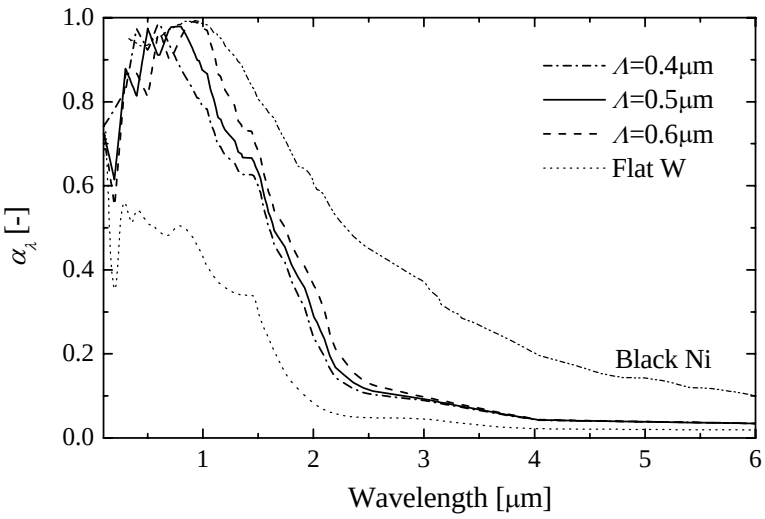

Fig. 4.

Sai et al.

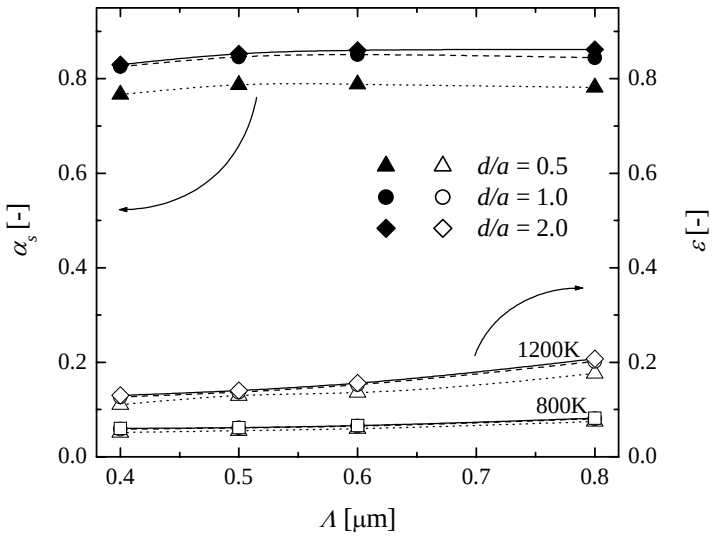

Fig. 5.

Sai et al.

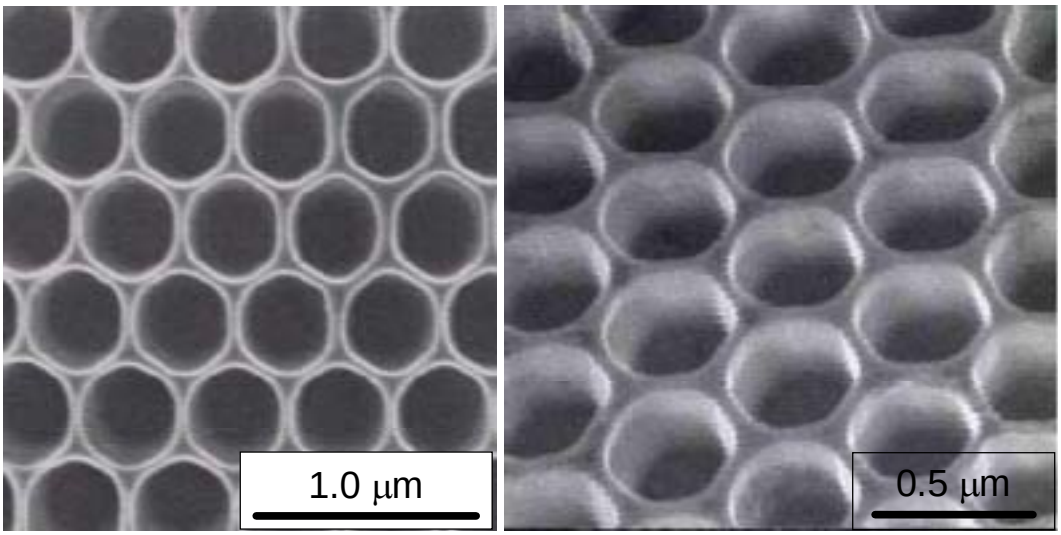

Fig. 6.

Sai et al.

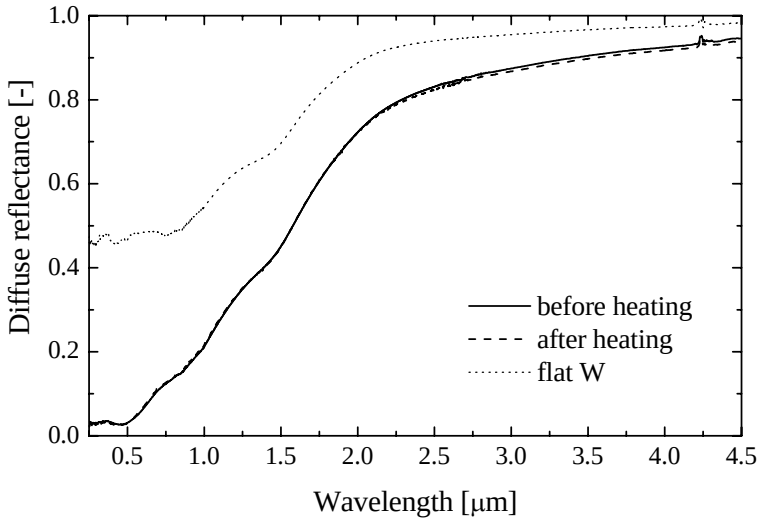

Fig. 7.

Sai et al.

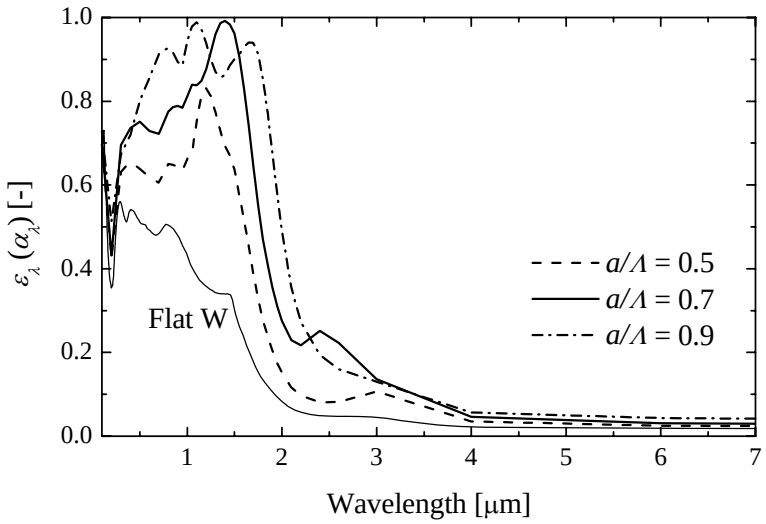

Fig. 8.

Sai et al.

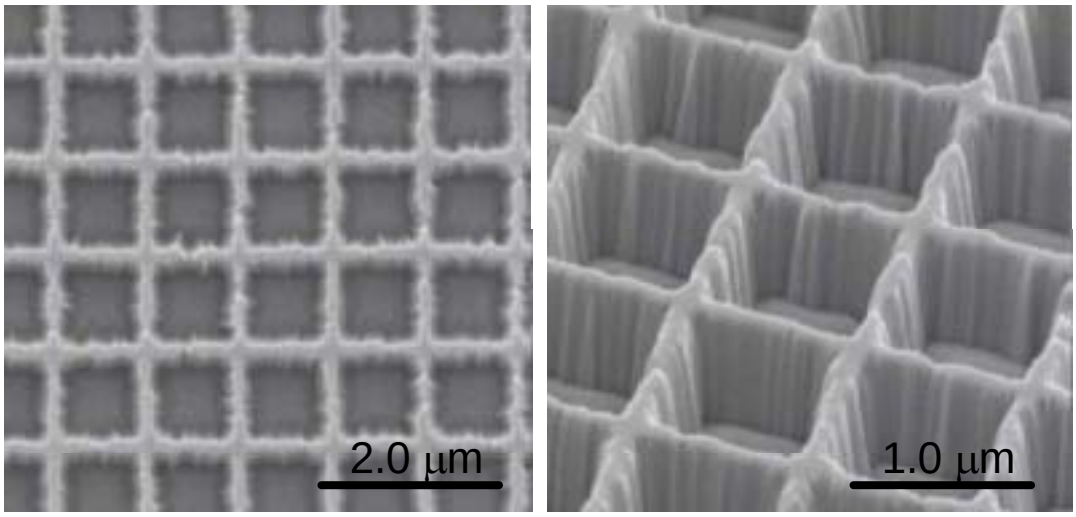

Fig. 9.

Sai et al.

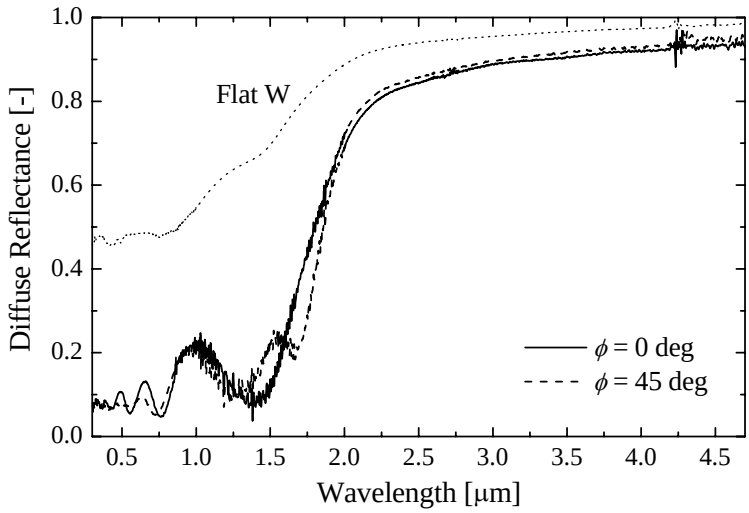

Fig. 10.

Sai et al.